

Large-scale low-energy excitations in 3-d spin glasses

Replica symmetry breaking and characterization in position space

J. Houdayer¹, F. Krzakala², and O. C. Martin²

¹ Institut für Physik, Mainz, Germany

² LPTMS, Univ. Paris-Sud, Orsay, France

October 29, 2018

Abstract. We numerically extract large-scale excitations above the ground state in the 3-dimensional Edwards-Anderson spin glass with Gaussian couplings. We find that associated energies are $O(1)$, in agreement with the mean field picture. Of further interest are the position-space properties of these excitations. First, our study of their *topological* properties show that the majority of the large-scale excitations are sponge-like. Second, when probing their *geometrical* properties, we find that the excitations coarsen when the system size is increased. We conclude that either finite size effects are very large even when the spin overlap q is close to zero, or the mean field picture of homogeneous excitations has to be modified.

PACS. 75.10.Nr Spin-glass and other random models – 75.40.Mg Numerical simulation studies

1 Introduction

The physics of spin glasses [13] is an old yet still very active subject of study. Much progress has been made in understanding the nature of the low temperature phase, but some fundamental issues remain open. Among these is whether the free-energy landscape consists of multiple valleys all contributing to the partition function in the thermodynamic limit. This is what happens in mean field theory [10], and a growing consensus is that it also arises in finite dimensions. Perhaps the strongest numerical evidence in favor of this comes from the spin overlap probability distribution $P(q)$ that seems to be non-trivial (see [9] for a review).

Several other striking properties of mean field may also hold in finite dimensions; the purpose of our work is to test this by numerically characterizing the valley states in the energy landscape of the 3-dimensional Edwards-Anderson [2] (EA) spin glass model. In the mean field picture, one expects some system-size excitations (configurations obtained from the ground state by flipping a finite fraction of all the spins) to have excess energies of $O(1)$. Furthermore, these excitations should (i) be sponge-like with non-zero surface to volume ratios; and (ii), be homogeneous on scales larger than the lattice spacing.

We first describe how we find excitations in Section 2 and then discuss in Section 3 some possible scenarios for how replica symmetry breaking may arise in position space (unfortunately sometimes called real space). In Section 4 we investigate topological properties of system-size excitations. Previous work [6] gave evidence that the $3 - d$

EA model with free boundary conditions had system-size excitations whose energies were $O(1)$. In the present work, we use periodic boundary conditions and consider the excitations' windings around the lattice to classify them topologically. We conclude again that it is possible to flip a finite fraction of all the spins at an $O(1)$ energy cost. Furthermore, most of these excitations are sponge-like, and our data are compatible with the possibility that *all* system-size excitations are sponge-like in the thermodynamic limit. Then in Section 5 we try to characterize the geometrical properties of these excitations. We measure their surface area and correlation functions, and then probe the distribution of their hole sizes. The data is most naturally interpreted as indicating that there is an intrinsic length scale that grows with the lattice size; if this scale grows indefinitely, then surface to volume ratios of the excitations go to zero [6,12] asymptotically. Beyond this scale (which is much smaller than the lattice size), excitations may be homogeneous, in agreement with the mean field picture. Given the small range in sizes that we can treat, it is also possible, though less likely, that the growth of this length scale is a finite size effect which saturates for larger sizes; if this is the case, the mean field picture holds and excitations are spongy beyond a few lattice spacings; whether they are homogeneous or lumpy is less clear as we find evidence for heterogeneities on scales much larger than the lattice spacing.

2 System-size excitations

2.1 Valleys

Consider a general Ising spin glass model with pairwise couplings

$$H = - \sum_{i < j} J_{ij} S_i S_j \quad (1)$$

Let N be the total number of spins. We would like to characterize the energy landscape of this system through the statistical properties of its valleys. In the infinite volume case, one can define a valley via the configuration at its bottom; the bottom of a valley can be defined as a minimum of the energy under all *finite* number of spin flips. Unfortunately, this simple definition has to be modified in finite volume; a simple yet heuristic modification consists in imposing the energy to be a minimum under any number of spin flips fewer than vN . $v \in [0, 1/2]$ is a distance parameter (in fact it is the Hamming distance divided by N) related to the usual spin overlap q by $q = 1 - 2v$. Because of the global spin flip symmetry of the Hamiltonian, hereafter we will force $q \geq 0$.

The influence of v on the definition of the valleys is important as all valley bottoms by construction will differ by at least vN spin flips. Suppose one had a 1-step replica symmetry breaking with a spin overlap probability distribution

$$P(q) = \alpha \delta(q) + (1 - \alpha) \delta(q - q_1) \quad (2)$$

If $q_1 \rightarrow 1$ as the temperature goes to zero, all choices of v satisfying $v < 1/2$ would recover the thermodynamically relevant valleys as $N \rightarrow \infty$. However, in the EA model, one expects the replica symmetry breaking to be continuous and valleys with overlaps arbitrarily close to 1 should arise in the zero temperature limit. Then any fixed choice of v will eliminate some of the thermodynamically relevant valleys. Since this effect decreases as v does, one could simply choose a small value of v and determine empirically the extent of the robustness in v of the analysis.

However from a numerical point of view, the main difficulty lies in *finding* low energy states rather than in classifying them. In fact, it is at present nearly impossible to find the minimum number of spins to flip before the energy of a configuration is lowered. Thus we cannot even tackle the task of finding the best valley lying within a reduced distance v and $(v + \Delta v)$ from the ground state. Because of this limitation, we have chosen a more hands-on approach where we just *sample* low-lying excitations. Given the way we find these configurations, we expect that nearly always they will in fact be bottoms of valleys.

2.2 Low energy excitations

From an algorithmic point of view, the ground state configuration \mathcal{C}^0 of a spin glass can be determined with a high level of confidence as long as N is not too large. In this work, we have used a genetic renormalization algorithm [4] which allows us to go to lattices up to 12^3 . Now

for extracting valleys or excited states, it is necessary to first compute \mathcal{C}^0 and then to introduce a \mathcal{C}^0 -dependent constraint or perturbation to the Hamiltonian that will lead to a modified ground state labeled \mathcal{C}^1 .

We have followed the constraint-based technique proposed in [6]: given the ground state, we flip the relative orientation of 2 selected spins and compute the new ground state with this constraint. A large scale excitation is obtained only if its energy is smaller than that of all the droplets surrounding either of the two selected spins. In practice, we repeat this multiple times by randomizing the choice of the two selected spins, obtaining a collection of \mathcal{C}^1 excitations. Note that this method gives no control over the number V of spins that will flip when going from \mathcal{C}^0 to \mathcal{C}^1 .

For each instance (set of J_{ij}), our numerical simulation then leads to \mathcal{C}^0 (the ground state), and a number of excitations. From this set, one can extract the configurations that satisfy any desired constraint. For instance, one may impose $V/N \geq v_{min}$ when looking for excitations of size growing linearly with N and study the energy and position space properties of these excitations.

2.3 Two scales for finite energy excitations

Hereafter, we consider only the three-dimensional Edwards-Anderson model with nearest-neighbor interactions. The J_{ij} are i.i.d. Gaussian random variables of zero mean and unit variance, and we work with $L \times L \times L$ cubic lattices ($L^3 = N$) and periodic boundary conditions.

Our procedure for sampling excitations can extract low energy droplets, but within the mean field picture one expects to also find large-scale excitations whose size grows *linearly* with N . We can test this two-scale picture by considering the probability distribution of V , the number of spins flipped when going from the ground state to the excited state. Suppose that the only excitations having $O(1)$ energy are the droplets (V finite as $L \rightarrow \infty$) and system-size excitations ($v = V/N$ finite as $L \rightarrow \infty$). Then excitations where $V \rightarrow \infty$ but $v \rightarrow 0$ as $L \rightarrow \infty$ will have a probability tending towards 0. Mathematically, this means that our extraction of excitations leads to a probability distribution for V of the form

$$P_L(V) \xrightarrow{L \rightarrow \infty} \alpha P_l(V) + (1 - \alpha) P_g(v) \quad (3)$$

where P_l and P_g are the normalized probability distributions associated with droplet (local) and system-size (global) excitations.

We have measured the frequencies of “events” with V for instance in the range $[L^2, 2L^2]$ as a function of L . (We say that we have an event in our data set whenever an instance and our sampling procedure lead to an excitation satisfying chosen criteria. Here and in the rest of our study, we generated three excitations for each instance; we have 10000 instances at each value of $L \leq 10$, 8000 at $L = 11$, and 5000 at $L = 12$.) The frequencies decrease with L and quite reasonably can be extrapolated to zero. As an example, for the interval given above, we

find the frequencies 0.520 ($L = 4$), 0.397 ($L = 5$), 0.321 ($L = 6$), 0.256 ($L = 7$), 0.232 ($L = 8$), 0.208 ($L = 9$), 0.187 ($L = 10$), 0.170 ($L = 11$), and 0.162 ($L = 12$). Note that by construction, one cannot get excitations whose energies are larger than those of droplets, so all states found in our sampling necessarily have $O(1)$ energies. This analysis then confirms the two-scale form given in equation (3).

3 Spin glass scenarios in finite dimensions

3.1 Length scales for self-averaging

Consider first the *energy* of system-size excitations. In the mean field picture (as motivated by the properties of the SK model) we expect to be able to find a \mathcal{C}^1 (for any choice of v_{min}) with a finite probability, and that its energy will be $O(1)$, i.e., finite when $N \rightarrow \infty$. On the contrary, in the droplet [3] and scaling [1] pictures, the characteristic energy of large scale excitations grows as a power of L . In [5] it was argued that one should distinguish the energy scaling of large-scale excitations from that of droplets in an infinite system; it is then necessary to introduce two exponents, θ_g (g for global) and θ_l (l for local); for instance the lowest system-size excitations have energies scaling as L^{θ_g} . Section 4.2 will lead us to the conclusion that $\theta_g \approx 0$. Extrapolating to finite temperature as is now commonly done [7], this indicates that replica symmetry is broken in the three-dimensional Edwards-Anderson model, i.e., the overlap probability distribution $P(q)$ is non-trivial in agreement with many previous studies (see [9] for a review).

Consider now the *position-space* characteristics of these large scale excitations. We are concerned here with the properties of the (connected) cluster of spins that are flipped when comparing to the ground state; we shall use the term *excitation* when referring to this cluster in addition to the configuration \mathcal{C}^1 itself. By definition, the sizes of these clusters are $O(N)$ (those are the events we focus upon). Of major interest is to understand whether these excitations are topologically non-trivial or not, homogeneous or inhomogeneous, fractal, multi-fractal, etc... To classify the different possibilities, we ask how the properties of the clusters depend on the scale of observation and on L , the size of the lattice. Clearly there are many observables that can be considered; to stay as simple as possible this discussion will focus on the cluster's density or equivalently on its local overlap as a function of the scale of observation.

Consider an $M \times M \times M$ window or box and let q_M be the overlap between \mathcal{C}^0 and \mathcal{C}^1 restricted to this box. (The cluster's density in the box is just $(1 - q_M)/2$.) Obviously q_M fluctuates no matter how large M is as the global overlap q itself is not self-averaging. But if we fix q , at what scale in M do the fluctuations in q_M disappear, or equivalently, what is the typical fluctuation of q_M as a function of the observation scale M ? Let $P_{M,L}(q_M)$ be the *disorder-averaged* distribution of q_M ; its mean is q and its variance will decrease to zero as M approaches L . We can

distinguish different scenarios according to the behavior of this distribution. We can expect and will assume that we have *pointwise* convergence in the infinite volume, i.e., that at fixed M

$$P_{M,L}(q_M) \xrightarrow{L \rightarrow \infty} P_M(q_M) \quad (4)$$

(Note that the global overlap between the two configurations must be fixed, and so this distribution depends implicitly on q .) It is possible that in fact this convergence will be *uniform* in the mathematical sense, that is one converges to the same function even if M varies with L . We then say that the limit is “regular”, leading to “regular” scenarios. The other scenarios will be non-regular, i.e., the convergence will be non-uniform. The key property that distinguishes these scenarios is whether or not q_M becomes self-averaging at a fixed (L -independent) scale. In the regular scenarios, the fluctuations in q_M disappear as M grows, so that the scale for self-averaging is a few (or many) times the lattice spacing. In the non-regular scenarios, $P_M(q_M)$ will not tend towards a delta function as $M \rightarrow \infty$; fluctuations will go to zero only when M is sufficiently big compared to an L -dependent scale.

In physical terms, the regular scenarios have no hidden scale; as soon as one takes large enough windows, one has convergence of q_M towards q in the probabilistic sense. As a consequence, once the global overlap q has been fixed, there are essentially no significant fluctuations in density down to a few lattice spacings, $P_{M,L}$ being very peaked about its mean. q_M is then self-averaging when q is fixed as soon as M becomes large compared to 1. On the contrary, in the non-regular scenarios, $P_{M,L}$ does not become peaked about its mean. For q_M to become self-averaging, one needs to go out to an L -dependent scale, for instance $M \approx L^\gamma$. A simple system that realizes this scenario is a ferro-magnet with anti-periodic boundary conditions; then $\gamma = 1$, and for scales $M \ll L$, $P_{M,L}$ has a two peak structure; q_M is not self-averaging on any scale smaller than L .

Our presentation has concentrated on the behavior of *density* fluctuations on different scales, but it generalizes in a straightforward manner to other observables (surface of the clusters, number of handles, etc...). Since different observables may become self-averaging on different scales, it is best to keep in mind that the complete picture may be more complicated than that obtained by looking at density fluctuations alone.

3.2 Two scenarios with uniform convergence

With *uniform* convergence, the limit $L \rightarrow \infty$ in equation 4 need not be restricted to M fixed; any M (dependent or not on L) will lead to the value given by the pointwise limit. We can say that there is a smooth or regular infinite volume limit on all scales simultaneously.

Our classification of regular scenarios is based on the way P_M converges towards a (single!) delta function as $M \rightarrow \infty$. Zooming into the region around its peak, one may expect P_M to have a limiting shape if we rescale the

x axis so that the full-width half-max stays constant. If the limiting shape, P^* , decays quickly so all moments exist, then fluctuations much larger than typical ones will be very rare and we will say that the system is homogeneous. If, on the contrary, P^* is a *broad* distribution, then rare events can dominate the mean square of density fluctuations, and we will say that the system is heterogeneous. Let us give physical pictures of these two cases.

Regular homogeneous sponges

Consider first the regular *homogeneous* scenario. A well known system having this behavior is the Ising model near its Curie point. Long wave-length fluctuations occur and decrease in intensity with wave-length. The dependence of this intensity on the scale (M) is not the point here, rather we focus on the *distribution* of the fluctuations at given M . In this physical system, fluctuation intensities much larger than the typical ones are very rare, the probability distribution P^* decays faster than any power. For our spin glass problem, we will have the regular homogeneous scenario if the density fluctuations of the clusters have this same property as long as we keep the global overlap q fixed. In a pictorial language, the clusters associated with an excitation will be rather random at scales larger than the lattice spacing, and can be thought of as homogeneous sponges characterized mainly by their density v and their effective mesh spacing ℓ_c . The terminology “sponge” comes from the fact that such objects are full of handles and are bicontinuous: they and their complement are connected, and the local density beyond the scale ℓ_c is nearly uniform. This length ℓ_c , called the cohesive length of the sponge [5], is just a few lattice spacings. (Since the convergence is uniform, the lattice spacing is the only scale, ℓ_c cannot diverge with L and it is unnatural for it to be many lattice spacings.)

Regular inhomogeneous sponges

A different scenario is obtained if we give up the homogeneity hypothesis. We still maintain uniform convergence of observables towards their large L limit, but now we assume that the density fluctuations arise not via low intensity modes but via holes in the sponges. To use the picture of Villain, we have something like a swiss cheese, except that the starting point is a sponge rather than the whole lattice, and from this we take out (or put in) blocks of contiguous spins. The resulting object is lumpy on all finite scales and the distribution of hole sizes and thus P^* has long tails. But as long as large holes are sufficiently rare, we can maintain the uniform convergence so that this lumpy system has no characteristic scale other than the lattice spacing.

The mean field picture

In any uniform convergence or regular scenarios, a finite fraction of the sites in the cluster are at a finite distance

from the cluster’s complement; thus the surface area of the cluster grows as L^3 , and the link overlap q_L cannot go to 1 as $L \rightarrow \infty$; $P(q)$ and $P(q_l)$ are *both* non-trivial, as in the SK model. Within mean field theory there is no intrinsic scale for self-averaging that grows with L , thereby suggesting that all observables converge uniformly to their limits; because of that, we shall hereafter simply say that the “mean field picture” corresponds to having uniform convergence of observables.

3.3 Scenarios without uniform convergence

In this class of scenarios, the $L \rightarrow \infty$ limit does not commute with the scale of observation (M) going to infinity. In other words, there is at least one L -dependent scale that affects the large L limit [7]. The simplest such case has a single scale (also called ℓ_c) such that the observable under consideration (for instance the local density) is self-averaging beyond ℓ_c and has a non trivial distribution below. When L is finite but large, $P_{M,L}(q_M)$ can be approximated by considering its difference with $P_M(q_M)$; it is natural to expect this difference to depend only on the ratio M/ℓ_c . We can then write

$$P_{M,L}(q_M) \underset{L \rightarrow \infty}{\approx} P_M(q_M) + A_1 f_{M/\ell_c}^1(q_M) \quad (5)$$

More generally, if there were many characteristic lengths ℓ_c^i , we could construct such an expression recursively by imposing the condition $f_0^i = 0$; the first term is always the pointwise limit, and the terms following give the correction associated with passing through the scale ℓ_c^i . Note that once a scale $M \gg \ell_c^k$ is reached where $P_{M,L}$ is a single delta function, then for observables such as density that involve additive quantities no further change in the distribution is possible.

In their full generality, these scenarios with multiple scales are quite complicated. Let us expose a few possibilities in the simplest case where there is a single ℓ_c . That scale must grow indefinitely with L , for instance as a power of L . Suppose now that $P_M(q_M)$ converges at large M to two delta function peaks centered at q_{min} and q_{max} , while if we take $M \gg \ell_c$ $P_{M,L}(q_M)$ converges to the single delta function peak at q (recall that beyond the scale ℓ_c , q_M becomes self-averaging and thus must equal the global overlap q). We have two simple candidate scenarios depending on q_{min} and q_{max} .

Fat sponges

If $q_{min} = 0$ and $q_{max} = 1$, then at finite scales one never sees the surface of the cluster, while at scales larger than ℓ_c the cluster is homogeneous so should resemble a sponge. (For this last property we assume $\ell_c \ll L$.) We call this case the “fat sponge” scenario as the clusters are just sponges whose characteristic mesh spacing is ℓ_c . Indeed, up to a dilation of the clusters, everything looks like the regular homogeneous scenario except that $\ell_c(L) \rightarrow \infty$ in the infinite volume limit.

We can consider several properties of such sponges. First, since the surface of the cluster does not grow as fast as its volume, the standard link overlap converges to a delta function at $q_l = 1$, and we have a scenario that realizes the TNT [6, 12] (trivial q_l , non-trivial q) behavior. Second, the nature of the cluster’s surface on scales smaller than ℓ_c will play an important role. The surface is unlikely to be smooth as in the ferromagnetic case; instead, it might be continuum fractal, having a fractal dimension $2 < d_f < 3$. But once one reaches the scale ℓ_c , everything becomes homogeneous as q_M becomes self-averaging.

Hierarchical sponges

Consider now the possibility that $q_{min} \neq 0$ and $q_{max} \neq 1$. Then below the scale ℓ_c one is in either of two phases differing in their density, but neither of these two phases resembles the ground state locally. In fact these two phases could resemble sponges, differing mainly by their densities. We will call this a “hierarchical sponge” scenario because one can produce such clusters by hierarchically applying sponge excitations to the ground state. Indeed, start with the ground state and create a fat sponge by flipping a spongy cluster whose characteristic mesh spacing is ℓ_c . Then if we take that state and flip a spongy cluster whose characteristic mesh spacing is $O(1)$, we find that there are locally only two densities and we obtain a two-step hierarchical sponge. (Naturally this construction can be generalized to any number of levels.)

Fractals

Consider the fat sponge scenario but take ℓ_c to grow linearly with L . Then there is no regime where $M \gg \ell_c$ and the cluster never becomes homogeneous. There is thus no reason to expect it to be sponge-like (although it may with a finite probability wrap around the lattice and have some of the topological properties that sponges have). The main motivation for this scenario is that it is what arises in a disordered ferro-magnet. Its characteristic is that q_M is not self-averaging until $M \rightarrow L$ and we can expect to get non-trivial distributions for observables such as q_M when M is a finite fraction of L .

Overall, we see that there is a great diversity of possible scenarios. Ideally our goal would be to test for the uniform or not convergence of observables as $L \rightarrow \infty$. However, from the point of view of the mean field picture, we shall be plagued by finite size effects, whereas from non-mean field viewpoints the results will be encouraging but still a bit muddled. The main conclusion will be that ℓ_c grows with L , i.e., the clusters coarsen as L grows. This coarsening may stop as in the mean field scenarios, or we may be seeing evidence in favor of the fat sponge scenario. But certainly ℓ_c does not grow linearly with L , ruling out the fractal scenario having heterogeneities on the scale L .

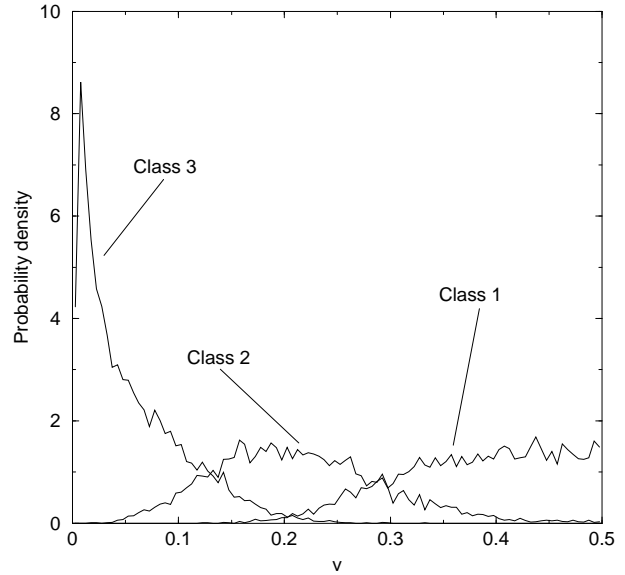


Fig. 1. Distribution of event sizes for $L = 10$, decomposed according to winding class type.

4 Topological properties

4.1 Classification by windings

Suppose we consider all events in our data set with $v = V/N$ in a given window; we then find that the relative frequency of these events *decreases* as L increases. Within the droplet model, this is expected, and in fact the frequency should decrease to zero as $L^{-\theta}$. On the contrary, in the mean field picture, that frequency should go to a constant non-zero value, and its decrease is interpreted as a finite size effect. Because θ is quite small, we cannot use that data alone to discriminate between these two pictures. Thus for each excitation we will also look at its topological properties as defined from the connected cluster of spins that are flipped in that excitation. Our motivation is if that there are system-size excitations of low energy, we expect them to be topologically non-trivial, and so a joint study of topology and v may allow one to extrapolate to $L \rightarrow \infty$ cleanly. Indeed, if the frequency of these types of events *grows* rather than diminishes as L increases, it becomes plausible that they survive in the thermodynamic limit.

Clearly a complete topological characterization of the clusters is not necessary. With free boundary conditions, it was possible [6] to limit oneself to finding out whether the cluster and its complement touched the different faces of the cube. Here, since we insist on maintaining periodic boundary conditions, we generalize that criterion by considering the winding properties of the cluster in the cube. Given a cluster, we determine whether there are paths on that cluster (going from site to nearest neighboring site) that wind around in any of the three directions (x, y, z) of the cubic lattice. From this, we define three classes of clusters as follows. A cluster (and thus the event and excitation) belongs to the first class if it *and* its complement

Table 1. Fraction of sponges and droplets

Size	Sponges	Droplets
4	0.230(3)	0.251(3)
5	0.253(3)	0.306(3)
6	0.271(3)	0.346(3)
7	0.284(3)	0.374(3)
8	0.290(3)	0.389(3)
9	0.300(3)	0.399(3)
10	0.304(3)	0.412(3)
11	0.302(4)	0.421(4)
12	0.310(5)	0.423(5)

have a non-trivial winding in all 3 directions of the cube. A cluster belongs to the third class if it has no windings at all. Finally, the second class consists of all other events. We will refer to events in the first class as sponges for obvious reasons, while events in the third class will be referred to as droplets.

4.2 Sponges with $O(1)$ energies

For each excitation obtained from an instance, we compute its overlap q with the ground state or equivalently its v , and determine to which topological class it belongs. Figure 1 gives the probability density of v for each of the three classes defined. The data represented is for 10000 different instances with $L = 10$, and for each instance we generated 3 excitations. The droplets (events in the third class) create a peak at small v while the other two classes are responsible for the rest of the distribution. Now to understand how these distributions evolve with L , we consider the total contribution of the different classes, integrated over v . From Table 4.2 we see that sponge (first class) events have an increasing frequency with L and so can reasonably be extrapolated to constitute a non-zero fraction in the large volume limit. This had also already been the case with free boundary conditions [6].

We feel that these data provide strong evidence that there are system-size excitations with $O(1)$ energies. Extrapolating to finite temperature, this leads to replica symmetry breaking in the 3d Edwards-Anderson model. Furthermore, because of the constraints built into the first class, these excitations span the whole system. From a direct visualisation of the clusters, we also see that their topology is highly non-trivial: they resemble sponges in that they have handles everywhere on a scale of a few lattice spacings. They are thus both space spanning (extending throughout the whole system) and space filling, at least on the scale of L .

4.3 Are all valleys sponge-like?

Given the data in Table 4.2, one can ask whether all low-energy system-size excitations asymptotically fall into the first class. In particular, if a uniform convergence scenario

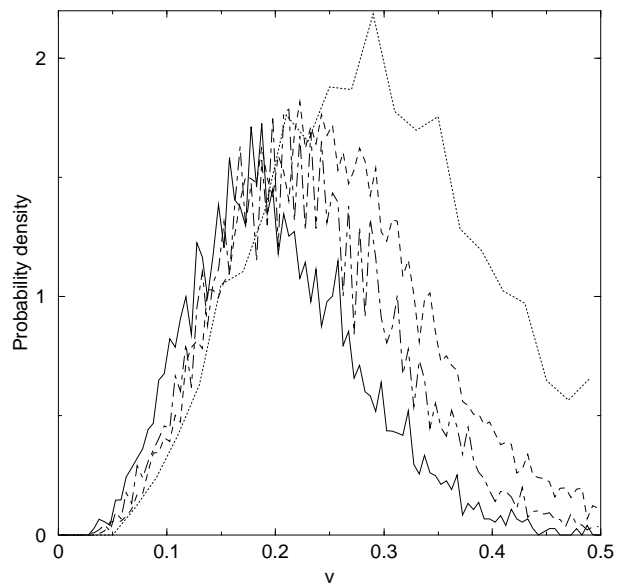


Fig. 2. Probability density of event sizes for $L = 4, 6, 8, 12$ from right to left; only the contribution of class 2 events are shown.

of spin glasses is correct, one expects to find only sponges in the thermodynamic limit as argued in [5], so that the second (intermediate) class should disappear when $L \rightarrow \infty$.

To see whether this is the case, we have studied the probability density of v as a function of L , decomposed according to the topological classes. The results for class 2 are displayed in figure 2. It shows that as L increases, the curves shift towards smaller v while the fraction of all events falling into class 2 (given by the area under each curve) decreases. That this fraction decreases is necessarily the case as we saw that the fractions of the other two classes grow with L . Can we extrapolate this fraction of class 2 events to zero as $L \rightarrow \infty$? We have performed fits of this fraction to the functions $a + b/L + c/L^2$ and $a + b/L^c$; both fits give reasonable χ^2 s and lead to values for a that are in reasonable agreement: 0.18(0.01) and 0.17(0.01). Taken at face value, these extrapolations indicate that the uniform scenarios are not correct. However, we believe that regardless of what the correct scenario is, finite size effects are subtle for class 2 events. To justify this, let us look again at the data.

In Figure 3 we show the fraction of class 2 events as a function of $1/L$ (top curve). Because of the positive curvature of this data, it seems likely that this class survives in the thermodynamic limit, confirming the conclusion drawn from the fits. But as argued in [5], it is difficult to create sponges in finite dimensions when L is smaller than a typical ‘‘cohesion’’ length ℓ_c that may be substantially bigger than one lattice spacing, especially if the dimension is not large. This effect should be much more severe for small v ; indeed in that limit, creating a spongy yet connected cluster requires the sponge to be very ‘‘thin’’, most of its sites being at its surface. The energy of such a sponge is likely to be high, and so our procedure for generating

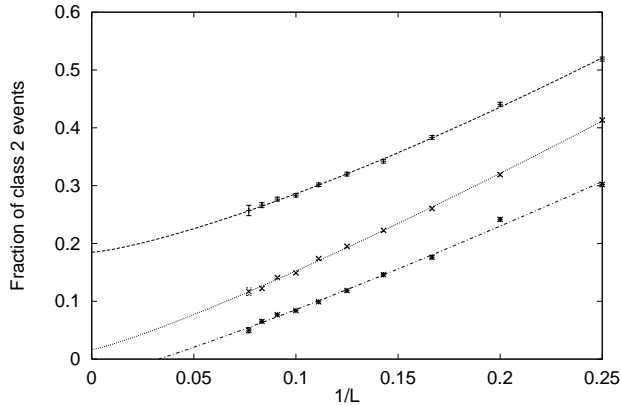


Fig. 3. Fraction of class 2 events and constant plus power fits. From top to bottom: case of $v > 0$, $v > 0.2$, and $v > 0.25$.

large scale excitations should not pick them up. We have explored the validity of this point of view by considering the fraction of class 2 events subject to a further selection in v . The three curves of Figure 3 are associated with the events satisfying $v > 0$, $v > 0.2$, and $v > 0.25$ (from top to bottom). We see that the fraction of these last events *cannot* be extrapolated to positive values, as confirmed by detailed fits. In fact, when we look at Figure 2, we can now reasonably assume that the curves all go to zero when L grows, but the smaller v is, the later the asymptotic behavior sets in. More convincing evidence of this is beyond the scope of our data, but we hope to have made the case that our results are not incompatible with class 2 events disappearing altogether in the large L limit.

In conclusion, great care is needed when performing extrapolations to large L because finite size effects are subtle when v is small. Therefore, in what follows, we will focus exclusively on the region near $v = 1/2$ ($q = 0$). If we are to provide any evidence that there is a growing length scale, it is only at $q \approx 0$ that such evidence can be solid.

5 Geometrical properties

We now move on to geometrical properties of low-energy system-size excitations: link overlaps, correlation functions, window overlaps, etc... From these measurements, we hope to test whether or not there is a growing intrinsic scale ℓ_c , and to thereby weight the balance in favor of some of the scenarios. Since spin glasses have resisted simple solutions, we do not expect the reader to find that any scenario comes out a clear winner but we do hope to convince her or him that the clusters coarsen significantly as L grows. Whether or not this coarsening continues to infinite sizes may be of fundamental importance; however, if it turns out that the growth is very slow, it should be of limited experimental relevance.

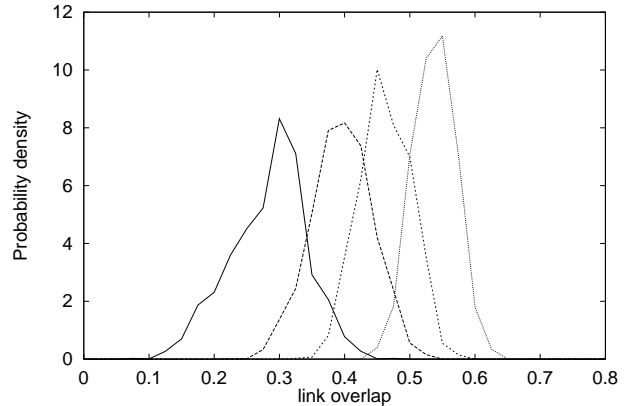


Fig. 4. Link overlap distributions for $L = 4, 6, 8, 12$. The data are for all events with $0 \leq q \leq 0.1$.

5.1 Mean link overlaps

We begin by considering the link overlap between the ground state and an excited state:

$$q_l = \frac{1}{3L^3} \sum_{i, \hat{\mu}} S^0(i) S^1(i) S^0(i + \hat{\mu}) S^1(i + \hat{\mu}) \quad (6)$$

We will take the surface S of the corresponding cluster to be the number of links that connect the cluster to its complement. Then we have $q_l = 1 - 2S/3L^3$. One of the main issues in this section is whether $q_l \rightarrow 1$ at large L , that is we want to know whether the system-size clusters have a surface to volume ratio that goes to zero at large L .

In the SK model, q_l is a deterministic function of the spin overlap q in the thermodynamic limit: $q_l = q^2$. An analogous deterministic relation will be satisfied in any scenario that is homogeneous on the length scale L . We can see whether this is the case in our system by considering the probability distribution of q_l at fixed q ; Figure 4 shows this distribution for different L values when $0 < q < 0.1$. (Note that for such small values of q , essentially all the excitations are sponge-like, i.e., fall into class 1 except for the smallest L s, and so a nearly identical plot is obtained if one restricts oneself to class 1 events.) Clearly the distributions are becoming more narrow with increasing L while drifting to the right. So we will look at both the mean and variance of these distributions.

In the uniform convergence scenarios the mean of these curves should settle at a $q_l < 1$ as $L \rightarrow \infty$ and so the drift is a finite size effect. On the contrary, in the fat sponge and fractal scenarios, the limiting q_l is equal to 1 and the drift is the signal that ℓ_c is increasing with L . (In the hierarchical sponge scenario, q_l should again converge to a value strictly smaller than 1.)

In geometrical terms, having $q_l \rightarrow 1$ means that the surface to volume ratios of the clusters go to zero at large L . Such a property was referred to as TNT in [6] as the link overlap q_l then has a trivial probability distribution [12] (it is infinitely narrow and localized at $q_l = 1$) while the distribution of the spin overlap q remains non-trivial.

We can try to discriminate between such different scenarios by performing fits, but it is necessary to parametrize the dependence of the mean on L for each scenario. Suppose that the asymptotic behavior of a quantity is L^α ; then we postulate that the finite size effects are multiplicative, with a finite size correction given by a function $f(1/L)$ where the argument is simply the ratio of the two scales of the problem, i.e., the lattice spacing and the lattice size. It is natural to assume that f can be Taylor expanded for small arguments, so we shall parametrize all our finite size effects by polynomials in $1/L$.

In TNT scenarios, one expects $\langle q_l \rangle - 1$ to go to zero as an inverse power of L , whereas in the scenarios with uniform convergence $\langle q_l \rangle - 1$ goes to a strictly positive constant. We have performed fits for these two types of scaling behavior. (We have also considered the possibility that $\langle q_l \rangle - 1$ vanishes as an inverse power of the logarithm of L , but the results are not convincing.) Consider first the fits having *two* free parameters. There is a linear fit in $1/L$, and a pure power fit, $\langle q_l \rangle - 1 = a/L^\gamma$, as shown in figure 5. We do not include the $L = 4$ data when fitting, and obtain χ^2 's of 67 and 19.5 for the two fits. (If instead we do leave the point at $L = 4$, the χ^2 's are increased to 149 and 49.) It seems plausible that we need to allow for more parameters and finite size corrections. So we allow now for three fitting parameters. The new χ^2 's are 7.5 and 6.3. This same pattern is repeated when one goes on to 4 free parameters. Certainly the case of a power law in L leads to the best fits and so is favored by the data. However, this advantage is only significant for the two parameter fits. (Note that when repeating all the fits after restricting the events to belong the sponge class, we find similar results.) Since it is quite possible that our parametrizations do not capture correctly the finite size effects, we cannot rule out the scenarios where $\langle q_l \rangle$ does not go to 1. Even so, it is worrisome that the asymptotic $\langle q_l \rangle$ values predicted by such scenarios drift with the number of parameters in the fits: we obtain $\langle q_l(L = \infty) \rangle = .68, .72$, and $.75$ for the fits with 2, 3, and 4 parameters.

To have a completely convincing test, we would need to have a range in L where only one of the fits gave χ^2 's that were close to the theoretically expected value. As can be seen in the figure, such a situation may not be so far: it might be enough to go to sizes up to $L = 16$ to finally obtain a clear cut discrimination of the different scenarios. In the mean time, we shall simply say that the TNT scenarios are slightly preferred.

Regardless of the scenario favored by the reader, perhaps the most striking point made here is that $\langle q_l \rangle$ undeniably increases for the currently accessible values of L , and that this is most simply interpreted by having ℓ_c growing with L . In models without geometry ℓ_c is small (for instance in the SK it is 1) whereas it seems to be at least 4 here even if we stick to the uniform convergence scenarios and identify ℓ_c with $1/(1 - q_l)$.

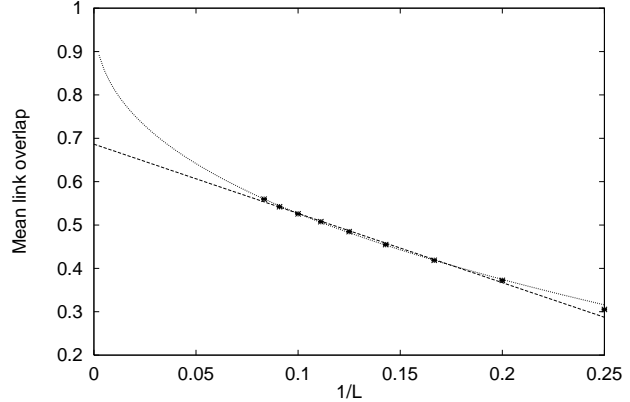


Fig. 5. Mean link overlap for excitations with $0 < q < 0.1$. Shown are fits for constant and power law asymptotics.

5.2 Variance of link overlaps

We come back now to the way the distribution of q_l becomes narrow. If the lattice spacing is the only relevant scale as in the homogeneous sponge scenario, we can expect $P(q_l)$ to converge to a delta function following the central limit theorem scaling law:

$$\langle (q_l - \langle q_l \rangle)^2 \rangle \approx CL^{-3} \quad (7)$$

However the data very clearly shows that $\langle (q_l - \langle q_l \rangle)^2 \rangle \times L^3$ grows tremendously with L and we see no way this can be compatible with finite size corrections to a constant asymptotic value. On the contrary, a fit to a power law looks sensible and we find that $\langle (q_l - \langle q_l \rangle)^2 \rangle \times L^{1.1}$ has no trend with L . This value for the exponent of the scaling of the variance of q_l is not very different from the value found by Marinari and Parisi [8] who extracted excitations in a very different way. This scaling suggests to us that there is an underlying length ℓ_c that diverges with L and that the density of the cluster's interface fluctuates on scales much larger than the lattice spacing. We also have measured the kurtosis of the distribution; we find that it does not decrease with L , showing explicitly that there is no central limit behavior. Overall, we feel that these results rule out the homogeneous sponge scenario for which the central limit theorem should hold. However we have nothing to say concerning the heterogeneous sponge scenario which can very well violate the central limit theorem.

5.3 Spin overlap correlation functions

Now we focus on the two-point correlation function defined by:

$$G(L, r) = \langle S^0(i)S^1(i)S^0(i+r)S^1(i+r) \rangle \quad (8)$$

We present in figure 6 this correlation function, as usual for events with $0 < q < 0.1$. We see again that finite size effects are very severe, making it quite difficult to guess what is the limiting curve when $L \rightarrow \infty$. In the regular

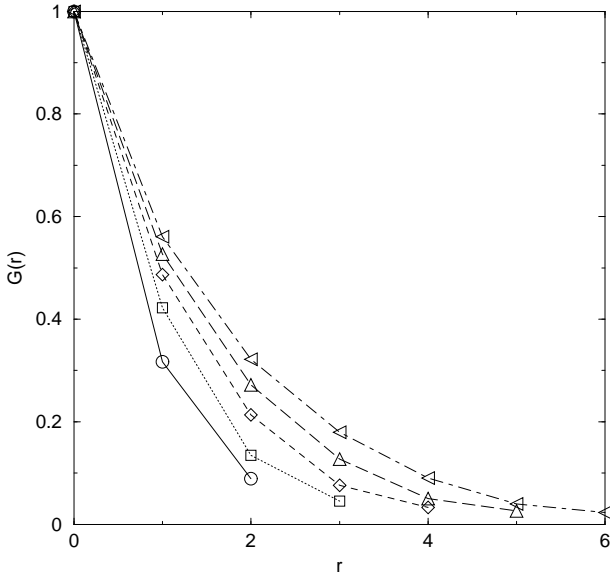


Fig. 6. Spin overlap correlation function at $0 < q < 0.1$ for $L = 4, 6, 8, 12$ (bottom to top).

scenarios, one expects $G(r, L)$ to converge to a limiting curve with for instance $1/L$ corrections, just as we saw for the mean link overlaps. For the TNT scenarios, the limiting curve is $G(r, L \rightarrow \infty) = 1$, and we can follow the discussion of finite size effects for $\langle q_l \rangle$ to motivate those of $G(r, L)$. (Note in particular that $G(1, L) = q_l$.) Since $G(r, L)$ probes properties at distance r , we will postulate in the fat sponge scenario that the finite size effects can be parametrized through

$$G(r, L) = 1 - A(r)L^{-\delta} \left(1 + \frac{B_1(r)}{L} + \dots \right) \quad (9)$$

in the region $r \ll \ell_c$, while $G(r, L)$ should be constant and equal to q^2 for $r \gg \ell_c$.

We have performed these fits. Since it was possible to fit reasonably well $G(1, L)$ to a constant different from 1 plus $1/L$ corrections, (cf. the previous section), it will be no surprise to find out that this remains true of $G(2, L)$. The difference between the $r = 1$ and $r = 2$ cases is that now the quality of the fits with $G(r, L = \infty)$ equal to 1 or less than 1 are similar, no scenario is favored. We have also tried to see whether a simple scaling law of the type $G(r, l) = G(r/L^\delta)$ might hold, but given the small useful range in r , no solid conclusion can be drawn. However, there should be a large usable range in r if we assume $G(r, l) = G(r/L)$ as in the fractal scenario. When we try that rescaling the data do not superpose at all: the large L curves that were above are now far below the others. There seems no way to avoid the conclusion that the correlation function data unambiguously rule out fractal scenario.

5.4 Window overlaps

Now consider the probability $P(M, L)$ that a cubic box of size M is entirely contained either in the cluster or in its

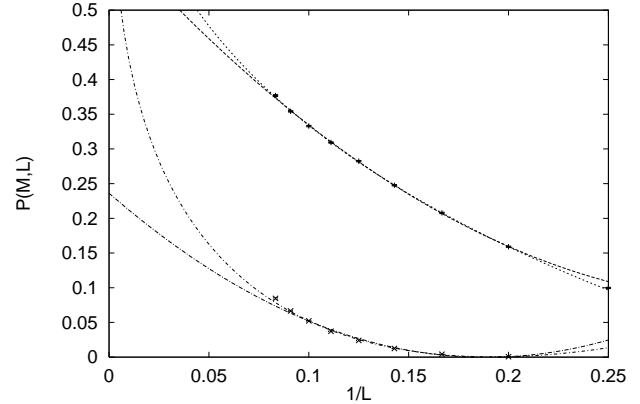


Fig. 7. Probability and fits that an M^3 box does not cross the surface of a cluster for $0 < q < 0.1$ events. Top: $M = 2$; bottom: $M = 3$.

complement. $P(M, L)$ has been studied in previous work, in particular by Palassini and Young [11]. Figure 7 gives these probabilities for our excitations at $M = 2$ and 3 for the window $0 < q < 0.1$. In any TNT scenario and in particular in the fat sponge scenario, $P(M, L) \rightarrow 1$ as $L \rightarrow \infty$ at any fixed M . We have performed the fits to this quantity in the same way as previously. The mean field picture is associated with polynomial fits in $1/L$, while in the fat sponge scenario we take

$$P(M, L) = 1 - A(M)L^{-\delta} \left(1 + \frac{B_1(M)}{L} + \dots \right) \quad (10)$$

For $M = 2$, we find the following χ^2 s for these two pictures: 311 and 10.6 for two free parameters, 14.4 and 7.5 for three free parameters, and 8.4 and 7.2 for four free parameters. (The same pattern transpires if we include the $L = 4$ data.) So here we seem to find more convincing evidence that the fat sponge scenario is significantly favored over the uniform convergence scenarios. The same study at $M = 3$ leads to the same conclusion, i.e., that the fat sponge scenario is favored.

5.5 Tube observables

In the context of the fat sponge scenario with a length scale ℓ_c , we may expect $P(M, L)$ to be a function only of the reduced variable $M/\ell_c(L)$. Unfortunately, the usable range in M is small (the data at $M = 4$ is not exploitable), and so the scaling cannot be reliably tested. This leads us to consider other observables that may have a larger useful range.

Rather than increase the size of the window in all three directions, we increase it in just one direction; because of this, we refer to these windows as “tubes”. We have investigated four different types of cross-sections for these tubes, as displayed in figure 8. Essentially, we use these objects to probe the size of holes in the clusters as follows. Given a tube type and a lattice site, we ask for the length of the longest tube along the x axis that passes through

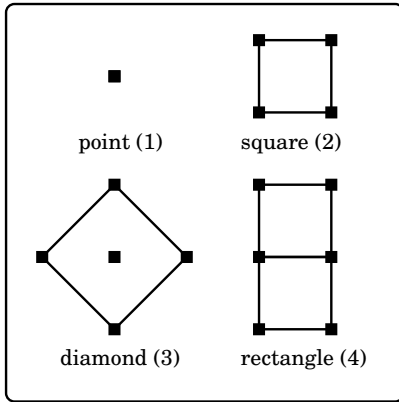


Fig. 8. The cross-sections of our four types of tubes.

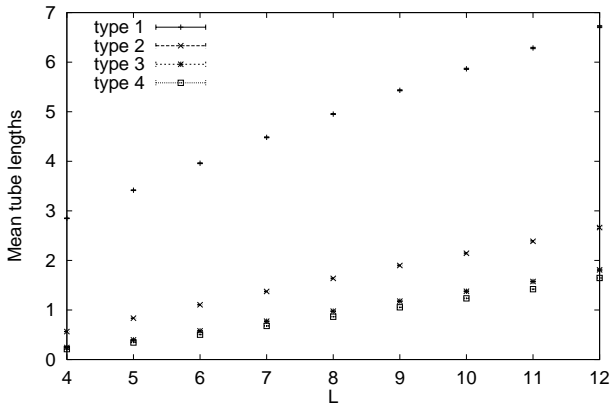


Fig. 9. Mean tube length for events with $0 < q < 0.1$ as a function of L .

this site and is entirely contained in the cluster (or in its complement). We compute this length for each site of the lattice and for the four different tube types. Then we extract the mean length found, averaged over lattice sites and over the disorder.

In figure 9 we see that the mean tube length increases very clearly as L increases, even for events with $0 < q < 0.1$. Within the fat sponge scenario, this is simply the reflection of the growth of ℓ_c with L . Is such a behavior compatible with the heterogeneous sponge scenario (having uniform convergence)? If the distribution of hole sizes is broad in heterogeneous sponges, the first moment may no longer be finite, leading to a divergence in the mean tube length. It is thus necessary to look directly at the probability distribution of these lengths. In Figure 10 we show the distribution of the tube lengths for tubes of type 2. (Tubes of type 1 show a much more severe drift with L , and the other tube types are quite similar to the one displayed.) We see that as L increases, the curves shift to the right while the values at small l decrease. In the uniform convergence scenarios, these distributions have a limiting shape, while in the fat sponge scenario for instance, the values at any finite l will go to zero. We have fitted the first three values ($l = 0, 1, 2$) in the figure as we have previously, i.e., to a finite or null asymptote, using

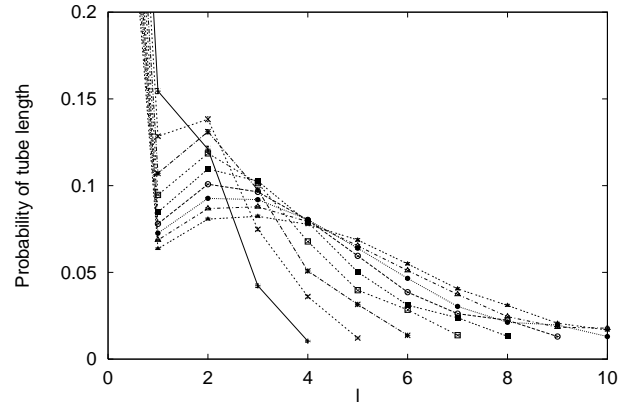


Fig. 10. Histogram of type 2 tube lengths for events with $0 < q < 0.1$, for $4 \leq L \leq 12$.

the data with $L > 5$. The fits at $l = 0$ have the same kind of behavior we saw before, i.e, the best fit is the extrapolation to zero, but the pure $1/L$ fit should not be excluded. (For two parameter fits, the χ^2 s are 27 for a non-zero extrapolation and 8.6 for the zero extrapolation; for the 3 and 4 parameter fits the zero extrapolations remain the best but are only marginally better than the ones for non-zero extrapolation.) For $l = 1$ and 2, there is no trend, but the extrapolated values are always very small, being below 0.03 and often ten times smaller than that. This result could have been guessed at from looking at Figure 10. Naturally, given the form of these histograms, it is much too difficult to extrapolate the data for still larger values of l , but nevertheless our conclusion is that the data do not support a point-wise convergence to a non-trivial distribution. At face value, this means that the uniform convergence scenarios are incorrect.

We can also look at the tail of the distribution. If $L \gg \ell_c$, we can expect the tail of the histogram to fall to zero rather rapidly with L . In practice though, we find that the histogram at $l = L$ grows with L for the tube types 3 and 4 for all values explored, while it first grows then decreases very slowly for type 2 tubes. At the very least, this is totally unexpected within the uniform convergence scenarios. Because of this, we have investigated the probability that a cluster has somewhere a tube of maximum length (that is of length L , the tube spanning the whole system along the x direction). We find that for tubes of the first type, 99% of the instances have at least one spanning tube, and that this ratio does not seem to depend on L . For the other tube types, we have collected the ratios in table 5.5. One sees that the ratios all increase with L . If we take into account the data for tubes of the first type, we are lead to extrapolate these ratios to finite quantities, distinct from 0 and 1. This goes strongly against the idea that the clusters are homogeneous beyond $\ell_c \ll L$. Indeed, in such a picture, the probability of having a tube span the whole system decreases exponentially. Here we need the decrease to be power-like so it can be compensated by the L^2 places where the tube can be located. Thus we are driven to a rather heterogeneous

Table 2. Fraction of excitations having a spanning tube

L	Tube 2	Tube 3	Tube 4
4	0.137(7)	0.006(2)	0.008(2)
5	0.22(1)	0.028(4)	0.020(3)
6	0.32(1)	0.080(6)	0.043(5)
7	0.38(1)	0.119(8)	0.080(6)
8	0.41(1)	0.15(1)	0.11(1)
9	0.46(1)	0.18(1)	0.13(1)
10	0.47(1)	0.22(1)	0.17(1)
11	0.48(1)	0.25(1)	0.20(1)
12	0.51(2)	0.28(2)	0.24(2)

picture (in the sense discussed in Section 3.2) where large fluctuations on scales larger than ℓ_c are possible, being suppressed by powers of L rather than exponentially in L/ℓ_c .

6 Conclusions

The only truly compelling property that emerges from this study is that the clusters coarsen as L grows. Naturally, this can be interpreted within the uniform scenarios as being a finite size effect; the issue is whether this is believable given the size of this effect. In essentially all the measurements we have made, the fat sponge type picture was favored over the homogeneous sponge scenario by a detailed χ^2 analysis. Furthermore as we saw from the tube observables, heterogeneities are large, so a scenario that is homogeneous on the scale of the lattice spacing seems ruled out. (We also saw for instance from the measurements of $G(r, L)$ that the scenarios where L is the only relevant scale are not supported by the data.) So our conclusion is mainly that the scenarios at the end of the spectrum (homogeneous regular sponge and fractal or droplet-like model) are no longer compelling. We are thus left with uniform convergence scenarios having large heterogeneities, and scenarios with at least one scale ℓ_c growing with L . In the first case, we have large finite size corrections because of the heterogeneities, while in the second we can realize the TNT scenario where q_l has a trivial distribution in the thermodynamic limit.

The difficulty of the problem should be all the more evident from the focus of our study: essentially all of our measurements were for the region $q \approx 0$. Obviously there is room for much more heterogeneities when q is larger. Nevertheless we hope to have shed new light on the problem of replica symmetry breaking in finite dimensional systems. And, as we have pointed out before, a convincing test of the major scenarios may not be so far off: we believe it is enough to go to slightly larger systems before the tests will become clear-cut to a vast majority.

Acknowledgments

We thank J.-P. Bouchaud and M. Mézard for very stimulating discussions and for their continuous encour-

agement. J.H acknowledges financial support from the Max Planck Institut, F.K. a fellowship from the MENRT, and O.C.M. support from the Institut Universitaire de France. The LPTMS is an Unité de Recherche de l'Université Paris XI associée au CNRS.

References

1. A. J. Bray and M. A. Moore. Scaling theory of the ordered phase of spin-glasses. In J. L. van Hemmen and I. Morgenstern, editors, *Heidelberg Colloquium on Glassy Dynamics*, volume 275 of *Lecture Notes in Physics*, pages 121–153, Berlin, 1986. Springer.
2. S. F. Edwards and P. W. Anderson. Theory of spin-glasses. *J. Phys. F*, 5:965–974, 1975.
3. D. S. Fisher and D. A. Huse. Equilibrium behavior of the spin-glass ordered phase. *Phys. Rev. B*, 38:386–411, 1988.
4. J. Houdayer and O. C. Martin. Renormalization for discrete optimization. *Phys. Rev. Lett.*, 83:1030–1033, 1999. cond-mat/9901276.
5. J. Houdayer and O. C. Martin. A geometrical picture for finite dimensional spin glasses. *Euro. Phys. Lett.*, 49:794–800, 2000. cond-mat/9909203.
6. F. Krzakala and O. C. Martin. Spin and link overlaps in three-dimensional spin glasses. *Phys. Rev. Lett.*, 85:3013–3016, 2000. Cond-mat/0002055.
7. E. Marinari and G. Parisi. Effects of changing the boundary conditions on the ground state of Ising spin glasses. *Phys. Rev. B*, 62:11677, 2000. cond-mat/0005047.
8. E. Marinari and G. Parisi. On the effects of a bulk perturbation on the ground state of 3d Ising spin glasses. 2000. cond-mat/0007493.
9. E. Marinari, G. Parisi, F. Ricci-Tersenghi, J.J. Ruiz-Lorenzo, and F. Zuliani. Replica symmetry breaking in short range spin glasses: A review of the theoretical foundations and of the numerical evidence. *J. Stat. Phys.*, 98:973, 2000. cond-mat/9906076.
10. M. Mézard, G. Parisi, and M. A. Virasoro. *Spin-Glass Theory and Beyond*, volume 9 of *Lecture Notes in Physics*. World Scientific, Singapore, 1987.
11. M. Palassini and A. P. Young. Triviality of the ground state structure in Ising spin glasses. *Phys. Rev. Lett.*, 83:5126–5129, 1999. cond-mat/9906323.
12. M. Palassini and A. P. Young. Nature of the spin glass state. *Phys. Rev. Lett.*, 85:3017, 2000. cond-mat/0002134.
13. A. P. Young, editor. *Spin Glasses and Random Fields*. World Scientific, Singapore, 1998.